Cai *et al. Radiation Oncology* (2024) 19:181
https://doi.org/10.1186/s13014-024-02574-8

Radiation Oncology

RESEARCH

Open Access

Longitudinal dynamic MRI radiomic models for early prediction of prognosis in locally advanced cervical cancer treated with concurrent chemoradiotherapy

Chang Cai[1,2], Ji-Feng Xiao[3,4], Rong Cai[1,2], Dan Ou[1,2], Yi-Wei Wang[1,2], Jia-Yi Chen[1,2*] and Hao-Ping Xu[1,2*]

Abstract

Purpose To investigate the early predictive value of dynamic magnetic resonance imaging (MRI)-based radiomics for progression and prognosis in locally advanced cervical cancer (LACC) patients treated with concurrent chemoradiotherapy (CCRT).

Methods and Materials A total of 111 LACC patients (training set: 88; test set: 23) were retrospectively enrolled. Dynamic MR images were acquired at baseline (MRI_{pre}), before brachytherapy delivery (MRI_{mid}) and at each follow-up visit. Clinical characteristics, 2-year progression-free survival (PFS), and 2-year overall survival (OS) were evaluated. The least absolute shrinkage and selection operator (LASSO) method was applied to extract features from MR images as well as from clinical characteristics. The support vector machine (SVM) model was trained on the training set and then evaluated on the test set.

Results Compared with single-sequence models, multisequence models exhibited superior performance. MRI_{mid}-based radiomics models performed better in predicting the prognosis of LACC patients than the post-treatment did. The MRI_{pre}-, MRI_{mid}- and the ΔMRI_{mid} (variations in radiomics features from MRI_{pre} and MRI_{mid}) -based radiomics models achieve AUC scores of 0.723, 0.750 and 0.759 for 2-year PFS and 0.711, 0.737 and 0.789 for 2-year OS in the test set. When combined with the clinical characteristics, the ΔMRI_{mid}-based predictive model also performed better than the other models did, with an AUC of 0.812 for progression and 0.868 for survival.

Conclusion We built machine learning models from dynamic features in longitudinal images and found that the ΔMRI_{mid}-based model can serve as a non-invasive indicator for the early prediction of prognosis in LACC patients receiving CCRT. The integrated models with clinical characteristics further enhanced the predictive performance.

Keywords Cervical cancer, Concurrent chemoradiotherapy, Prognosis, Radiomics, Machine learning

*Correspondence:
Jia-Yi Chen
chenjiayi0188@gmail.com
Hao-Ping Xu
xhp11701@rjh.com.cn
Full list of author information is available at the end of the article

Introduction

Cervical cancer is the fourth most common malignant tumor and the fourth leading cause of cancer death among women worldwide [1]. According to all the latest international society guidelines, concurrent platinum-based chemoradiotherapy (CCRT) followed by intrauterine brachytherapy (BT) is the treatment of choice recommended for locally advanced cervical cancer patients (FIGO 2018 stages IB3-IVA) [2, 3]. However, the 5-year disease-free survival rate remains 52–68% and 5-year overall survival rate remains 54–73% [4], with most deaths due to subsequent systemic failure of distant metastatic disease [5], whereas the 5-year local control has improved with the introduction of MRI-based image-guided radiotherapy [6].

Several new strategies for combined treatment, including additional chemotherapy and novel agents such as PD-1/PD-L1 inhibitors, are under evaluation to improve the prognosis of locally advanced cervical cancer (LACC) patients [7–9]. The OUTBACK trial, aimed to determine the effects on survival of adjuvant chemotherapy given after standard cisplatin-based chemoradiotherapy, showing the additional chemotherapy did not significantly improve overall survival or progression-free survival in unselected LACC compared with concurrent chemoradiotherapy alone [8]. Similarly, the CALLA trial showed that durvalumab (PD-L1 inhibitor) concurrent with chemoradiotherapy was well tolerated in participants with LACC, while it did not significantly improve progression-free survival in a biomarker unselected population [9]. Meanwhile, as PD-L1 was recognised as a biomarker for response to immune checkpoint inhibitors in recurrent or metastatic cervical cancer during CALLA, the PFS benefit was evident in the PD-L1 TAP 20% or greater population regardless of LN involvement, which reminded that more biomarkers are needed to identify who will benefit from the the additional treatment.

In the studies mentioned above, it was noted that the study arms experienced an increased incidence of grade 3 and 4 toxicities, along with treatment-related deaths. However, the patients who experienced severe adverse effects from additional systemic treatment did not realize corresponding improvements in prognosis.

Thus, early identification of patients with high-risk disease who are likely to benefit the most from additional treatment is necessary, thereby avoiding the overtreatment of patients who respond well to standard-of-care treatments.

Clinical factors such as FIGO stage, histological type, and lymph node status are known to influence the prognosis of LACC patients. However, their predictive value is limited. In recent years, significant advancements in radiomics hold the promise of discovering non-invasive biomarkers. Such advancement could enable clinicians to deliver personalized anticancer treatments to each patient [10].

We hypothesize that dynamic MRI changes before and after early treatments, such as external beam radiotherapy (EBRT), may serve as predictors of survival in cervical cancer patients receiving concurrent chemoradiotherapy. Currently, no radiomics study has accurately predicted the prognosis of these patients at such an early treatment stage. Our study aimed to determine the optimal and earliest timing for predicting the prognosis of LACC patients and to develop a dynamic MRI-based radiomics predictive model before or early during treatment. This approach has the potential to improve overall survival rates by enabling the early implementation of intensive treatments for high-risk LACC patients.

Materials and methods

Patients

This study was performed with data from anonymized patients who received radiotherapy treatment between March 2017 and December 2021. The Institutional Ethics Committee of Ruijin Hospital approved this retrospective study (Date: 20,240,628, Reference Number: 2024-192). The requirement for written informed consent from each patient was waived because of the retrospective nature of the study. A total of 313 LACC patients were treated with CCRT at Ruijin Hospital, 111 of whom were retrospectively enrolled in this study (Fig. 1). The inclusion criteria were as follows: (1) histologically confirmed invasive carcinoma of the cervix; (2) FIGO 2018 stage IB3–IVA; and (3) treated with CCRT at Ruijin hospital. The exclusion criteria were as follows: (1) received neoadjuvant chemotherapy prior to CCRT; (2) underwent surgery following

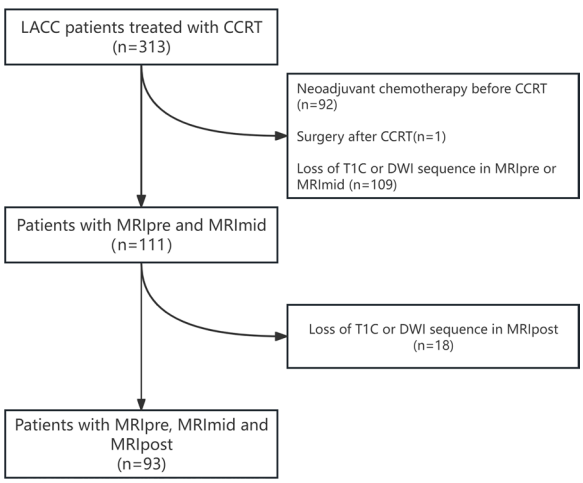

Fig. 1 Flowchart of patients included and excluded from this study

CCRT; and (3) lacked T1C or DWI sequences before CCRT or between EBRT and brachytherapy.

All patients underwent pelvic enhanced MRI, including T1C and DWI at baseline (MRI_{pre}), and before brachytherapy was delivered (MRI_{mid}). The MRI_{mid} was performed after EBRT but before brachytherapy in our clinical practice, allowing for precise radiation dose optimization.

Clinical characteristics such as age; maximum tumor diameter (MTD); lymph node metastasis; and involvement of the vagina, rectum, uterine corpus or bladder at diagnosis were recorded at baseline. The follow-up was conducted every 3 months during the first 2 years after treatment, every half-year for 3–5 years, and once a year thereafter. Patients were required to undergo MRI imaging during their routine follow-up. In this study, "MRI_{post}" referred to the MR images acquired 6 months after treatment. We observed the outcomes of the patients in the study via 2-year progression-free survival (PFS), which was defined as the period from the completion of CCRT to the first instance of locoregional recurrence or distant metastasis, and 2-year overall survival (OS), which was defined as the period from the completion of CCRT to death. LASSO regression was used to select the clinical factors associated with 2-year PFS and 2-year OS.

Image acquisition and segmentation strategy

All patients underwent pelvic MRI, which included both T1C and DWI with b values ranging from 700 to 1500 s/mm^2. The patients were imaged on a 1.5-T MR system at Ruijin hospital in DICOM format and converted into NIFTI format for subsequent analyses. MRI acquisitions were performed on a clinical 1.5 T MRI scanner (Siemens MAGNETOM Area 1.5 T MRI scanner). The main imaging parameters were as follows: (1) Axial T2WI: TR 4000 ms, TE 78 ms, number of slices 25, slice thickness 5 mm, FOV 250 mm × 250 mm, some were fat suppression sequences; (2) Axial DWI: TR 5300 ms, TE 74 ms, number of slices 26, slice thickness 5 mm, FOV 380 mm × 380 mm. with b values ranging from 700 to 1500 s/mm^2; (3) Axial DCE: TR 4.57 ms, TE 1.72 ms, slice thickness 4 mm, FOV 300 mm × 300 mm. Gd-DTPA was used as contrast agent at a dose of 20 mL and a flow rate of 2 mL/s. Arterial phase, venous phase and equilibrium phase images are obtained at 20–50 s, 1–2 min, and 2–3 min respectively. Then delayed axial images were acquired.

Regions of interest (ROIs) were manually delineated on each slice obtained from the T1C and DWI images by the same radiation oncologist to ensure reproducibility; then, the ROIs were validated by a senior radiation oncologist with at least 10 years of experience to ensure the accuracy of the tumor segmentation. The ROIs were drawn along the margin of the tumor on each slice of the axial contrast-enhanced MRI and DWI images. Areas of degeneration, hemorrhage, necrosis and exudation were included in ROI. The delineation and subsequent analyses were performed via the open-access software ITK-SNAP 3.8 (www.itksnap.org). A segmentation example is shown in Fig. 2.

Workflow of prognosis modelling

The radiomics workflow included six steps, as illustrated in Fig. 3. In this study, we included data from 111 cervical cancer patients, each with pre-treatment and mid-treatment DWI and T1C sequence MR images. The data were randomly divided at a ratio of 8:2, with 88 cases allocated to the training set and 23 to the test set. The ROI for feature extraction was manually outlined by radiation oncologists based on the GTV of the patients. For each set of patient data, we separately extracted 842 radiomics features and computed feature changes by subtracting the pre-treatment features from the mid-treatment features. These feature changes were then utilized as inputs, and the optimal feature set for classification prediction tasks was selected via LASSO regression. On the basis of the chosen optimal features, we conducted separate machine learning models on the DWI and T1-enhanced sequences via fivefold cross-validation. The output results of the two models were subsequently weighted and integrated to produce the final classification outcome. In this study, we assessed the predictive performance of SVM models and evaluated the classification performance of the models via ROC curves and area under the curve (AUC) values during the model testing phase.

Radiomics feature extraction

Radiomics features were automatically derived using the PyRadiomics open-source Python library. These features were computed from regions of interest (ROIs) on DWI and T1C sequence MR images representing pre-treatment and mid-treatment data, respectively. We calculated the feature changes by subtracting the mid-treatment features from the pre-treatment features for both the DWI and T1C data, thus obtaining the feature changes as inputs for the model. The computed features included first-order statistics, 3D morphology-based features, and texture analysis features such as Gray Level Cooccurence Matrix (GLCM), Gray Level Run Length Matrix (GLRLM), Gray Level Size Zone Matrix (GLSZM), Gray Level Dependence Matrix (GLDM), and Neighboring Gray Tone Difference Matrix (HGTDM). These features were extracted from both original images and images processed with wavelet filtration, employing both low-pass (L) and high-pass (H) wavelet filters. In our study, radiomics features were extracted in 3D,

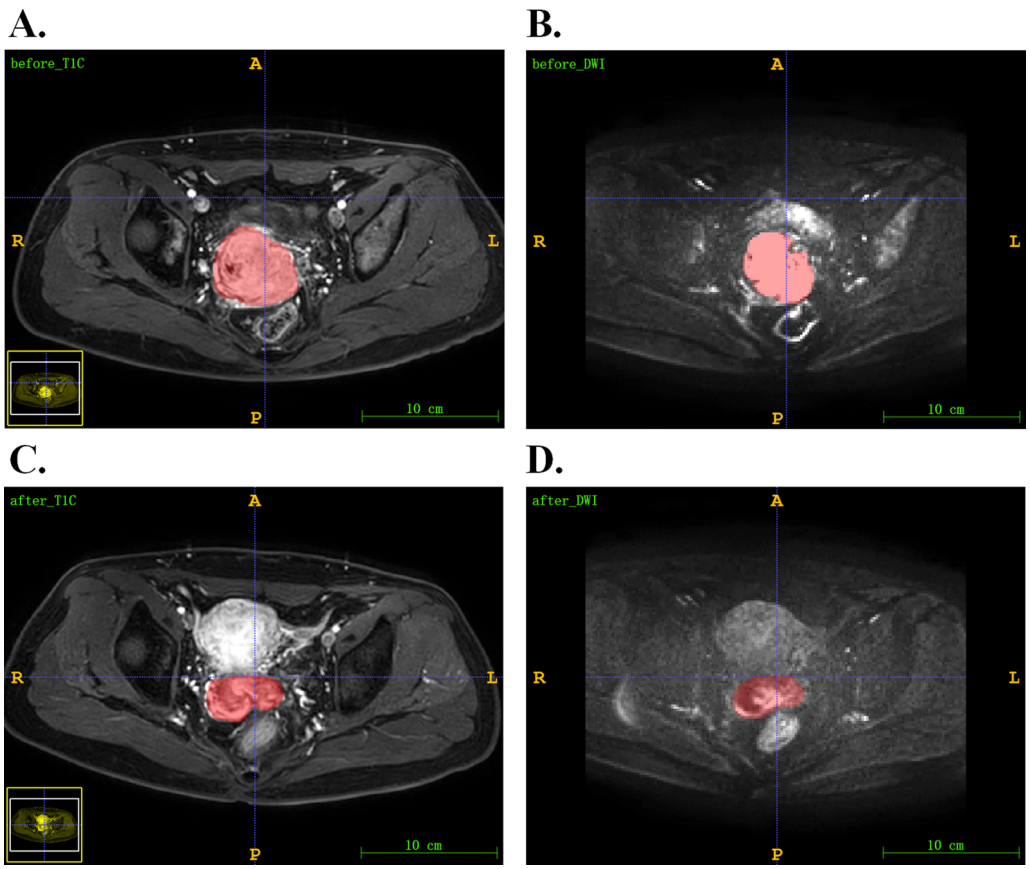

Fig. 2 The segmentation example using MR images in one patient. Pre-treatment MRI_{pre} T1C sequence (**A**) and DWI sequence (**B**), mid-treatment MRI_{mid} T1C sequence (**C**) and DWI sequence (**D**)

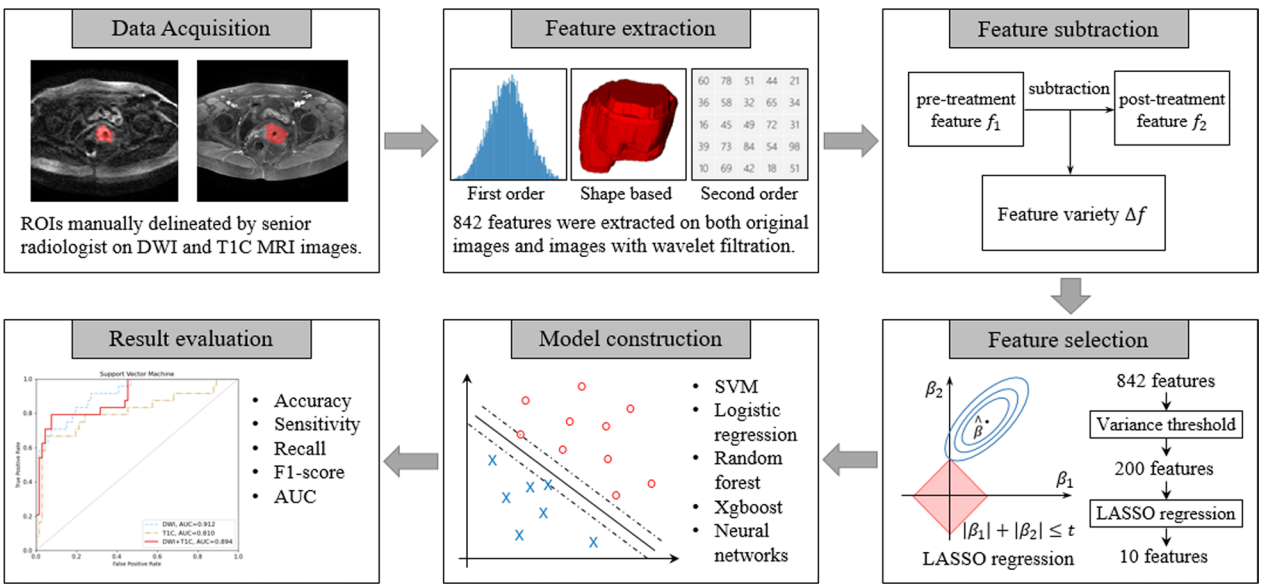

Fig. 3 Radiomics workflow for predicting the prognosis of patients with cervical cancer treated with CCRT

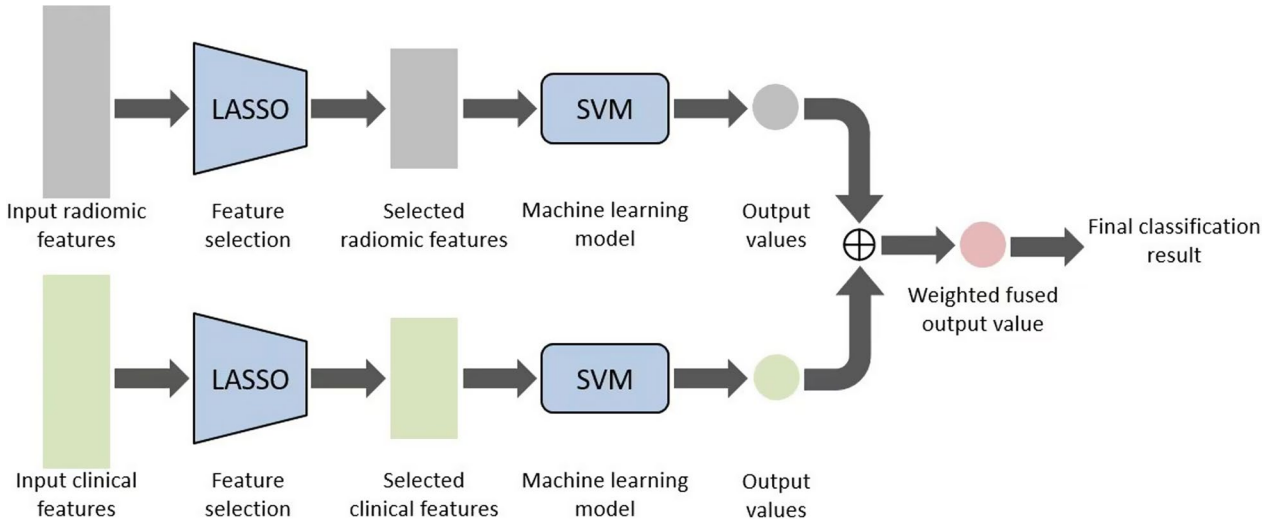

Fig. 4 The process of integrating radiomics features and clinical characteristics. Radiomics features and clinical characteristics were each processed through independent feature selection and machine learning modeling workflows to yield output probability values. These values were then multiplied by their respective weights and summed to obtain the fused probability value. Finally, the classification result was determined based on a predefined threshold

resulting in wavelet features computed across the x-, y-, and z-axes. The features were classified into eight distinct groups based on wavelet filtration patterns: wavelet-HLL, wavelet-LHL, wavelet-LHH, wavelet-LLH, wavelet-HLH, wavelet-HHH, wavelet-HHL, and wavelet-LLL.

Feature selection

To select the best features for prediction, we employed the variance threshold selection and least absolute shrinkage and selection operator (LASSO) logistic regression analysis, utilizing the open-source Python library Scikit-learn. During the feature selection phase, we initially filtered out features with a variance greater than 1 from a pool of 842 input features. Subsequently, these features were fed into LASSO regression for further refinement, resulting in the selection of the top 10–20 features most optimal for the prediction task. We used a fivefold cross-validation method for feature selection, which means that we input 80% of the training data's features into LASSO regression for selection every time and repeated this process five times to complete one fivefold validation selection. We repeated this process 100 times and recorded the 20 features that appeared most frequently as the final selected results.

Model construction and evaluation

In this research, we employed SVM as machine learning models to model and predict the selected features, all of which are based on the open-source Python library Scikit-learn. The features used to construct the classification model were not only the features of the DWI and T1C sequences but also their changes from pretreatment to mid-treatment. The optimal 10–20 features are selected through LASSO regression. For different MR image sequences, we modeled and predicted the DWI and T1C sequences separately and then performed weighted integration in the model output stage to obtain the final predicted classification results. We used a fivefold cross-validation method to optimize the parameters on the training set and then conducted model prediction performance tests on the pre-reserved test set. The predictive performance of the model was subsequently evaluated via the AUC of the receiver operating characteristic (ROC) curve.

Feature fusion

The machine learning models described above are built and trained using radiomics features extracted from DWI and T1C images in conjunction with clinical features. After individually modeling features from each imaging modality, the machine learning process integrated predictions through backend processing. This integration involved weighting and aggregating probabilities to derive a consolidated output value. Following this, classification occurred via weighted thresholds to determine the final decision based on the amalgamated classification outcomes. Importantly, the current fusion process was applicable solely to models employing the same machine learning algorithm; different machine learning models could not be combined. Ultimately, we evaluated the performance of models utilizing DWI features alone, T1C features alone, and a fused model that integrates

Table 1 The baseline clinical characteristics of patients enrolled in the study

Characteristics	Patients (n = 111)	Training set (n = 88)	Test set (n = 23)	*P* value
Age, years, median (range)	56 (28–84)	56 (28–84)	55(31–75)	0.603
Maximum tumor diameter (MTD), cm, median (IQR)	4.56 (3.95–5.2)	4.70(3.90–5.20)	4.30(4.00–5.08)	0.468
Histology (%)				0.600
Squamous cell carcinoma	106 (95.5)	85(96.6)	21(91.3)	
Others	5 (4.5)	3(3.4)	2(8.7)	
FIGO 2018 stage (%)				0.120
IIA	5 (4.5)	5(5.7)	0(0.0)	
IIB	34 (30.6)	26(29.5)	8(34.8)	
IIIA	11 (9.9)	7(8.0)	4(17.4)	
IIIB	6 (5.4)	3(3.4)	3(13.0)	
IIIC1	32 (28.8)	25(28.4)	7(30.4)	
IIIC2	17 (15.3)	16(18.2)	1(4.3)	
IVA	6 (5.4)	69(6.8)	0(0.0)	
Rectal involvement (%)				1.00
No	99 (89.2)	78(88.6)	21(91.3)	
Yes	12 (10.8)	10(11.4)	2(8.7)	
Bladder involvement (%)				1.00
No	95 (85.6)	75(85.2)	20(87)	
Yes	16 (14.4)	13(14.8)	3(13.0)	
Vagina involvement (%)				0.238
No	12 (10.8)	11(12.5)	1(4.3)	
Yes	99 (89.2)	77(87.5)	22(95.7)	
Upper 1/3	59 (53.2)	44(50.0)	15(65.2)	
Upper 2/3	16 (14.4)	15(17.0)	1(4.3)	
Lower 1/3	24 (21.6)	18(20.5)	6(26.1)	
Uterine corpus infiltration (%)				0.918
No	71 (64.0)	57(64.8)	14(60.9)	
Yes	40 (36.0)	31(35.2)	9(39.1)	
Parametrial invasion (%)				1.00
No	26 (23.4)	21(23.9)	5(21.7)	
Yes	85 (76.6)	67(76.1)	18(78.3)	
Lymph node metastasis (%)				0.374
No	56 (50.5)	42(47.7)	14(60.9)	
Yes	55 (49.5)	46(52.3)	9(39.1)	

DWI, T1C, and clinical features. The process of integrating radiomics features and clinical characteristics is illustrated in Fig. 4.

Results

Clinical characteristics

All patients underwent MRI, including T1C and DWI before and during CCRT at our institution. The median follow-up duration was 3.2 years (interquartile range [IQR] 2.2–4.6 years). The median age was 56 years (range 28–84 years), and the median MTD was 4.56 cm ([IQR] 3.95–5.20 cm). The baseline characteristics of the patients and the whole cohort are listed in Table 1. There were no statistical difference between training set and test set for each clinical characteristics.

All patients enrolled in this study received EBRT followed by brachytherapy. EBRT was delivered to the whole pelvis with photon beams at a daily dose of 1.8–2.0 Gy. Ninety-one of the 111 patients received concurrent weekly cisplatin-containing chemotherapy during EBRT.

After 2 years of follow-up, disease progression, including local/regional recurrences and distant metastases, occurred in 29 of the 111 patients (26.1%), whereas death

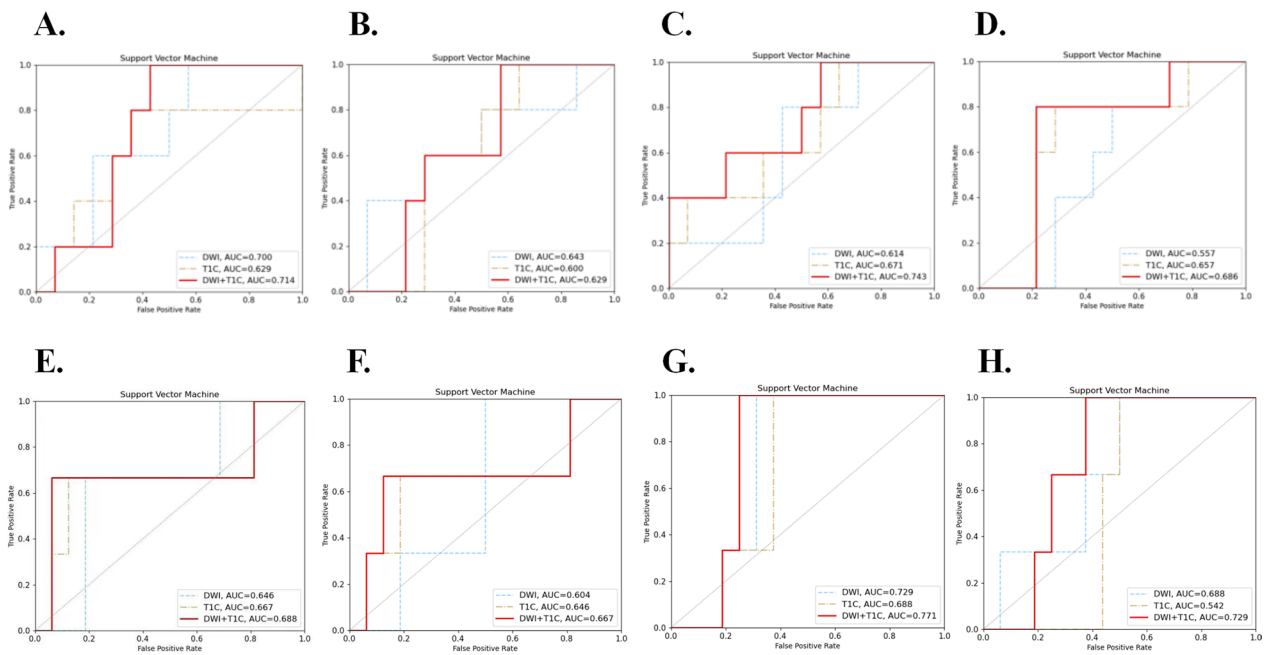

Fig. 5 ROC curves of models for the prognosis prediction of 2-year PFS and 2-year OS. ROC curves of models for the prognosis prediction of 2-year PFS (**A**–**D**): **A** MRI_{mid}-based models, **B** MRI_{post}-based models, **C** ΔMRI_{mid} (dynamic changes from MRI_{pre} to MRI_{mid}) based models, and D ΔMRI_{post-} (dynamic changes from MRI_{pre-} to MRI_{post})-based models. ROC curves of models for the prognosis prediction of 2-year OS (E ~ H): **E** MRI_{mid}-based model, **F** MRI_{post}-based model, **G** ΔMRI_{mid} (dynamic changes from MRI_{pre-} to MRI_{mid})-based model, and **H** ΔMRI_{post-}based model

was reported in 19 of the 111 patients (17.1%). Therefore, the 2-year PFS was 73.9%, and the 2-year OS was 82.9% in our study.

Radiomics models for different prediction timing: MRI_{mid} versus MRI_{post}

Initially, radiomics models were constructed based on 93 patients with MRI_{pre}, MRI_{mid} and MRI_{post} data, as shown in Fig. 1. For both 2-year PFS and 2-year OS, multi-sequence models achieved higher AUC scores than single-sequence models did. For 2-year PFS prediction, models based on MRI_{mid} performed better than models based on MRI_{post} (AUC score, 0.714[95%CI 0.590, 0.839] vs 0.629[95%CI 0.489, 0.768]), meanwhile the models based on dynamic changes from MRI_{pre} to MRI_{mid} (ΔMRI_{mid}) performed better than those based on dynamic changes from MRI_{pre} to MRI_{post} (ΔMRI_{post}) (AUC score, 0.743[95%CI 0.624, 0.861] vs 0.686[95%CI 0.555, 0.816]). For the 2-year OS prediction model, the AUC score was also greater for the MRI_{mid}-based model than for the MRI_{post}-based model (AUC score, 0.688[95%CI 0.535, 0.840] vs 0.667[95%CI 0.510, 0.824]) and for the ΔMRI_{mid}-based model than for the ΔMRI_{post}-based model (AUC score, 0.771[95%CI 0.642, 0.899] vs. 0.729[95%CI 0.588, 0.870]). The ROC curves for these models are shown in Fig. 5. The above results indicate that, compared with post-treatment timing, radiomics models based on early treatment timing perform better in terms of the prognosis of patients with LACC.

Performance of combining models for PFS and OS prediction

To improve the performance of the prediction models, the initial 111 patients were enrolled in the following analysis. A total of 842 radiomics features were extracted from both original and wavelet-filtered images. The optimal features for classification prediction tasks were selected via LASSO regression, as shown in Fig. 6. The details of features were shown in Supplementary Table 2 and Supplementary Table 3.

Similar results revealed that, compared with single-sequence models, multisequence models exhibited superior performance, achieving higher AUC scores on the test set. Models built with radiomic features from MRI_{pre}, MRI_{mid} and ΔMRI_{mid} achieved AUC scores of 0.723[95%CI 0.615, 0.831], 0.750[95%CI 0.647, 0.853] and 0.759[95%CI 0.658, 0.860] for 2-year PFS and 0.711[95%CI 0.583, 0.838], 0.737[95%CI 0.615, 0.858] and 0.789[95%CI 0.682, 0.896], respectively, for 2-year OS in the test set (Fig. 7).

Among the clinical characteristics, the influencing factors selected by LASSO regression for 2-year PFS in LACC patients were MTD, lymph node metastasis,

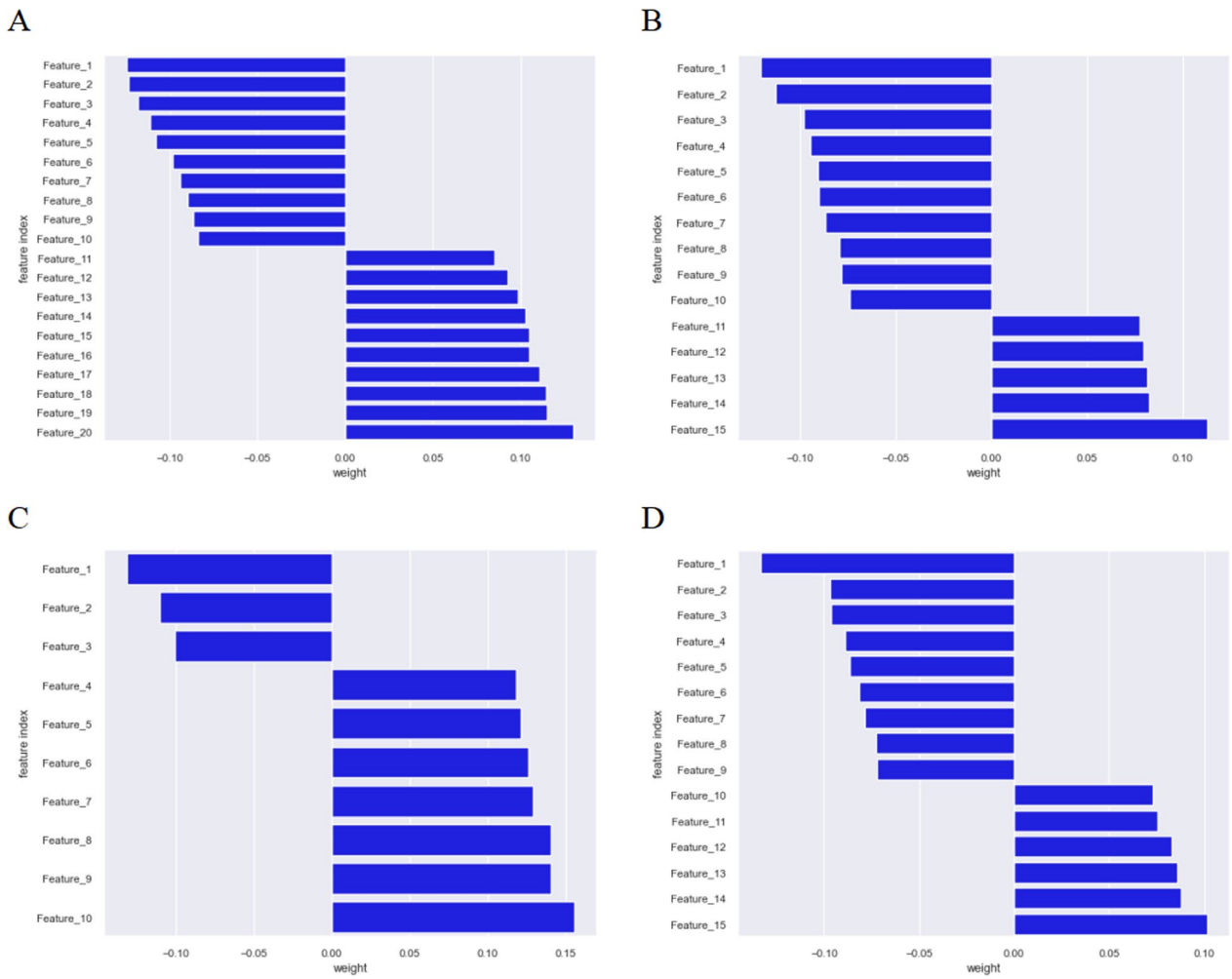

Fig. 6 Radiomics features selected by LASSO regression. **A** radiomics features extracted from the T1C sequence for 2-year PFS prediction; **C** radiomics features extracted from the DWI sequence for 2-year PFS prediction; **B** radiomics features extracted from the T1C sequence for 2-year OS prediction; **D** radiomics features extracted from the DWI sequence for 2-year OS prediction

vaginal and rectal involvement, age, and uterine corpus infiltration at diagnosis, and those for 2-year OS were MTD, lymph node metastasis, vaginal and rectal involvement, and bladder infiltration at diagnosis. The univariate analysis of clinical characteristics for progression-free survival and overall survival were shown in Supplementary Table 1.

When combined with these clinical characteristics above, the predictive model usingΔMRI_{mid} features achieved a higher AUC score than MRI_{pre} or MRI_{mid} model did, with an AUC of 0.812[95%CI 0.724, 0.901] for 2-year PFS and 0.868[95%CI 0.788, 0.948] for 2-year OS. Accuracy, specificity and recall of the combined models were 0.826, 0.875, 0.714 for 2-year PFS and 0.739, 0.737, 0.750 for 2-year OS. A comparison of the ROC curves for the different models is illustrated in Fig. 7.

Prediction scores for patient risk stratification

Figure 8 illustrates the composite prediction scores of our models for each patient in the training set and test set. The score of each patient is derived from the weighted fusion of imaging and clinical features via DWI and T1C images. Using the training set outcomes, we identify the optimal cut-off value for classification performance, which we then apply to categorize the test set outcomes. Based on the cut-off values for PFS (−0.032) and OS (0.053), patients can be categorized into high-risk and low-risk groups, respectively. For instance, locoregional recurrence and distant metastases are more likely to occur in patients in the high-risk group with the score value higher than the PFS cut-off value. The Kaplan–Meier curves are shown in Fig. 9.

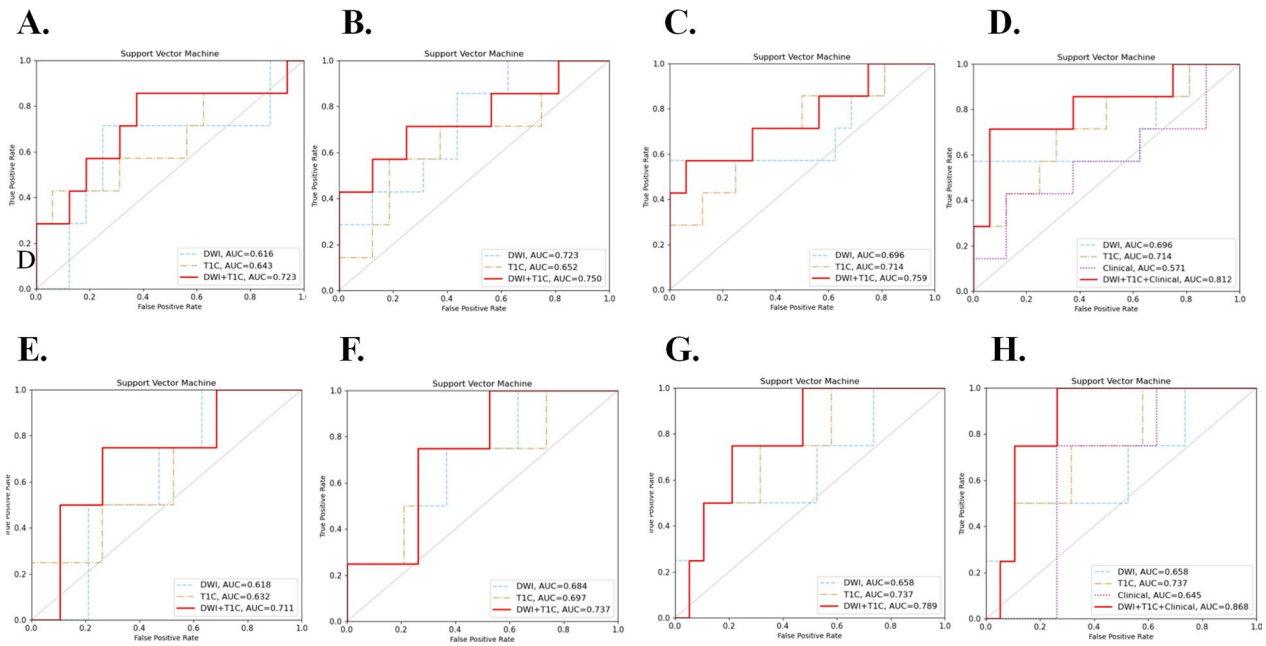

Fig. 7 Performance comparison of 2-year PFS and 2-year OS prediction models. 2-year PFS prediction models (**A**–**D**) **A** pre-treatment features **B** mid-treatment features **C** feature changes from pre-treatment to mid-treatment; **D**: radiomics feature changes + clinical features; 2-year OS prediction models (**E**–**H**) **E** pre-treatment features; **F** mid-treatment features; **G** feature changes from pre-treatment to mid-treatment; **H** radiomics feature changes + clinical features

Discussion

Our study demonstrated the feasibility of advancing the timing for predicting the prognosis of LACC patients from 6 months post-treatment to during treatment. This may provide a basis for appropriately adjusting the dose and fraction of subsequent brachytherapy, as well as for deciding whether to administer more intensive systemic treatments such as chemotherapy and immunotherapy. Additionally, we proposed predicting the prognosis of LACC patients by analyzing dynamic changes in radiomics features before and during treatment to achieve higher predictive performance.

Radiomics analysis has become a non-invasive method that visualizes and quantifies intratumoral heterogeneity by extracting high-throughput quantitative features from medical images, providing valuable prognostic information for medical decision-making. In recent years, researchers have used radiomics to predict response to neoadjuvant chemotherapy, efficacy, and outcomes such as PFS and OS in patients with locally advanced cervical cancer, primarily via MRI and PET-CT [11, 12]. Owing to its excellent soft tissue contrast and multiplanar capability, pelvic MRI is the most common imaging modality for evaluating locoregional tumor extent in cervical cancer patients [13] and was therefore applied in this study.

In previous studies, radiomics models that predicted the prognosis of LACC based on pre-treatment MRI consistently demonstrated excellent predictive performance [14–19]. These findings suggest that MR images contain information correlated with patient prognosis before treatment. For example, Zhang et al. successfully constructed radiomics models from pre-treatment MR images of 185 LACC patients, achieving C-index values of 0.762 for PFS and 0.750 for OS. The pre-treatment models in their study also exhibited excellent predictive performance, with AUC scores of 0.723 for PFS and 0.711 for OS in testing [14]. Most studies have shown that, compared with the use of radiomic models or clinical models alone, combining radiomics with clinical characteristics improves model performance [12, 20]. Therefore, we improved the predictive efficacy of our models by incorporating clinical characteristics, yielding results consistent with those of other studies (AUC scores of 0.812 for PFS and 0.868 for OS for testing).

The EMBRACE I study indicated that patients who did not achieve CR at 6–9 months had significantly worse outcome [21]. These findings suggest that imaging information at 6–9 months after treatment is sufficient to predict the prognosis of patients with LACC. In our study, the MRI_{mid}-based model demonstrated superior

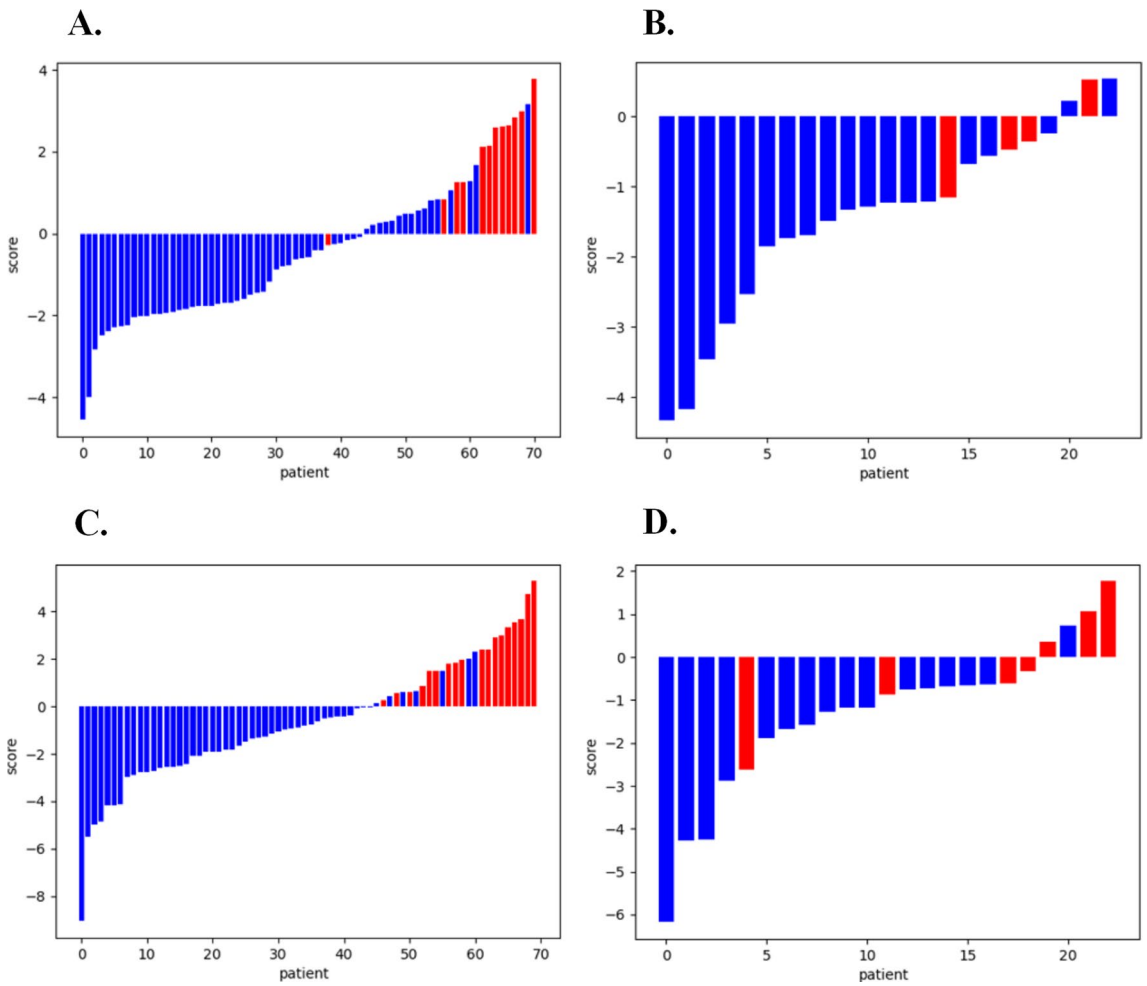

Fig. 8 Prediction outcomes of 2-year OS and 2-year PFS combined models. **A** training set for 2-year OS prediction; **B** test set for 2-year OS prediction; **C** training set for 2-year PFS prediction; **D** test set for 2-year PFS prediction

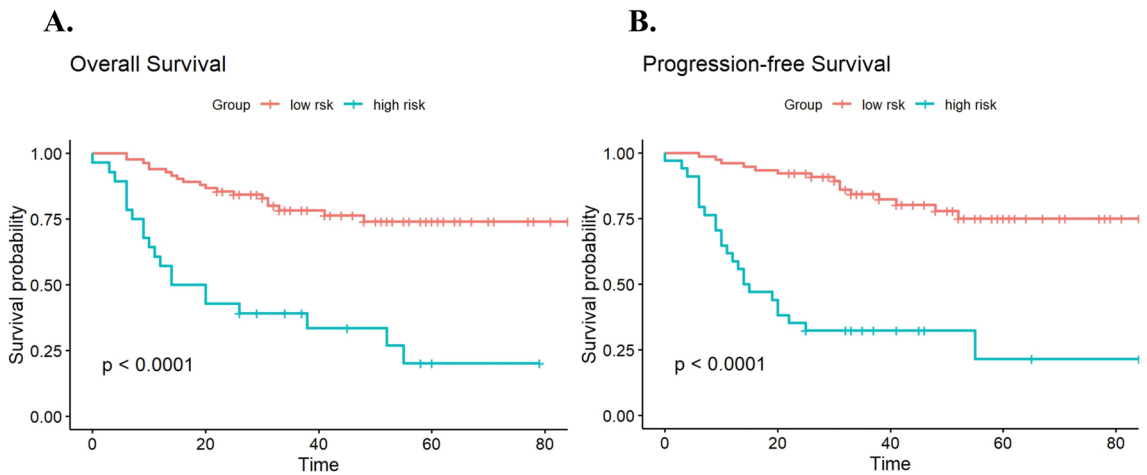

Fig. 9 Kaplan–Meier curves of the combined models for OS prediction (**A**) and PFS prediction (**B**)

predictive efficacy compared with the MRI_{post} model at 6 months after treatment. This finding indicates that it is unnecessary for patients to wait until the 6-month follow-up to predict future outcomes, enabling earlier adjustments to treatment intensity.

Solomon et al. reported that the response to neoadjuvant chemotherapy is associated with the prognosis of patients with esophageal cancer [22]. Similarly, Li et al. and Kong et al. confirmed that early clinical response to neoadjuvant chemotherapy in patients with cervical cancer can predict long-term survival [23, 24]. Current published research lacks a prognosis prediction model based on dynamic changes in MR images. This study proposes that a predictive model based on dynamic changes has advantages over one based on a single time point. The results of this study confirm this hypothesis, showing that radiomics models based on dynamic changes in MR data during early CCRT can predict the prognosis of LACC patients and even achieve better performance than models based solely on pre-CCRT MR images.

Although our radiomics-clinical models yielded satisfactory results, there are several limitations. First, our sample size is relatively small compared with that of other studies, and we did not utilize external validation cohorts, which may impact the generalizability of the model to real-world outcomes. In future research, we aim to optimize the predictive performance of the model and expand its application by leveraging larger patient cohorts from multiple centers. Second, this study employed a retrospective approach because of the need for a long follow-up time to assess PFS and OS, so the results require validation through prospective studies. Additionally, variability in patient image sequences led to the lack of MRI T2 sequences in this study. Although the radiomics models in this study exhibited comparable prognostic prediction performance to previously published models based on T2 sequences or their combinations [17, 18], the incorporation of T2 sequences in the future may enhance prognostic prediction performance and necessitate support from larger-scale studies.

In conclusion, the time point between EBRT and BT during treatment can serve as a non-invasive indicator for early prediction of prognosis in patients with LACC receiving CCRT. Additionally, the dynamic change in radiomics features before and after treatment offers better predictive performance. The findings of this study offer novel insights into predicting the prognosis of patients with LACC. By identifying high-risk patients early, intervention treatments can be administered promptly, potentially improving treatment outcomes. Moreover, patients with relatively better prognoses can avoid the toxicity of additional treatments. This approach holds promise for optimizing patient care in the future.

Abbreviations

MRI	Magnetic resonance imaging
LACC	Locally advanced cervical cancer
CCRT	Concurrent chemoradiotherapy
MR	Magnetic resonance
MRI_{pre}	MR images were acquired at baseline
MRI_{mid}	MR images were acquired before brachytherapy delivery
PFS	Progression-free survival
OS	Overall survival
LASSO	Least absolute shrinkage and selection operator
SVM	Support vector machine
ΔMRI_{mid}	Variations in radiomics features from MRI_{pre} and MRI_{mid}
BT	Brachytherapy
EBRT	External beam radiotherapy
DWI	Diffusion weighted imaging
MTD	Maximum tumor diameter
MRI_{post}	MR images acquired 6 months after treatment
ΔMRI_{post}	Variations in radiomics features from MRI_{pre} and MRI_{post}
ROIs	Regions of interest
AUC	Area under the curve
GLCM	Gray level cooccurence matrix
GLRLM	Gray level run length matrix
GLSZM	Gray level size zone matrix
GLDM	Gray level dependence matrix
HGTDM	Neighboring gray tone difference matrix
ROC	Receiver operating characteristic

Supplementary Information

The online version contains supplementary material available at https://doi.org/10.1186/s13014-024-02574-8.

Additional file 1 .

Acknowledgment
A part of this work is accepted as oral presentation at the ASTRO Annual Meeting2024, Washington, DC, USA

Author contribution
Jia-Yi Chen and Hao-Ping Xu made substantial contributions to the conception and conducteded this work. Chang Cai collected data, wrote the main manuscript text and prepared Fig. 1–2, 8. Ji-Feng Xiao was mainly involved in model building and prepared Fig. 3–7. Dan Ou, Yi-Wei Wang and Rong Cai interpreted the data and participated in formal analysis. All authors reviewed the manuscript.

Funding
This study was supported in part by Shanghai Science and Technology Innovation Action Plan (grant number 23Y41900100), the National Key Research and Development Program of China (grant number 2022YFC2404602), National Key R&D Program of China (grant number 2023ZD0502200), Shanghai Hospital Development Center Foundation (grant number SHDC12023108), Scientific and Technological Innovation Action Plan of Shanghai Science and Technology Committee (grant number 22Y31900103).

Data availability
In order to protect study participant privacy, original data in this work cannot be shared openly.

Declarations

Ethics approval and consent to participate
The Institutional Ethics Committee of Ruijin Hospital approved this retrospective study (Date: 20240628). The requirement for written informed consent from each patient was waived because of the retrospective nature of the study

Competing interests
The authors declare no competing interests.

Author details
[1]Department of Radiation Oncology, Ruijin Hospital, Shanghai Jiaotong University School of Medicine, Shanghai 200025, China. [2]Shanghai Key Laboratory of Proton-Therapy, Shanghai 201801, China. [3]Institute for Medical Imaging Technology, Shanghai 201800, China. [4]Shenzhen United Imaging Research Institute of Innovative Medical Equipment, Shenzhen 518048, China.

Received: 11 September 2024 Accepted: 17 December 2024
Published online: 21 December 2024

References

1. Sung H, Ferlay J, Siegel RL, et al. Global cancer statistics 2020: GLOBOCAN estimates of incidence and mortality worldwide for 36 cancers in 185 countries. CA Cancer J Clin. 2021;71(3):209–49. https://doi.org/10.3322/caac.21660.
2. Abu-Rustum NR, Yashar CM, Arend R, et al. NCCN guidelines® insights: cervical cancer, version 1.2024. J Natl Compr Canc Netw. 2023;21(12):1224–33. https://doi.org/10.6004/jnccn.2023.0062.
3. Cibula D, Pötter R, Planchamp F, et al. The European society of gynaecological oncology/European society for radiotherapy and oncology/European society of pathology guidelines for the management of patients with cervical cancer. Radiother Oncol. 2018;127(3):404–16. https://doi.org/10.1016/j.radonc.2018.03.003.
4. Mayadev JS, Ke G, Mahantshetty U, Pereira MD, Tarnawski R, Toita T. Global challenges of radiotherapy for the treatment of locally advanced cervical cancer. Int J Gynecol Cancer. 2022;32(3):436–45. https://doi.org/10.1136/ijgc-2021-003001.
5. Narayan K, Fisher RJ, Bernshaw D, Shakher R, Hicks RJ. Patterns of failure and prognostic factor analyses in locally advanced cervical cancer patients staged by positron emission tomography and treated with curative intent. Int J Gynecol Cancer. 2009;19(5):912–8. https://doi.org/10.1111/IGC.0b013e3181a58d3f.
6. Pötter R, Tanderup K, Schmid MP, et al. MRI-guided adaptive brachytherapy in locally advanced cervical cancer (EMBRACE-I): a multicentre prospective cohort study. Lancet Oncol. 2021;22(4):538–47. https://doi.org/10.1016/S1470-2045(20)30753-1.
7. Dueñas-González A, Zarbá JJ, Patel F, et al. Phase III, open-label, randomized study comparing concurrent gemcitabine plus cisplatin and radiation followed by adjuvant gemcitabine and cisplatin versus concurrent cisplatin and radiation in patients with stage IIB to IVA carcinoma of the cervix. J Clin Oncol. 2011;29(13):1678–85. https://doi.org/10.1200/JCO.2009.25.9663.
8. Mileshkin LR, Moore KN, Barnes EH, et al. Adjuvant chemotherapy following chemoradiotherapy as primary treatment for locally advanced cervical cancer versus chemoradiotherapy alone (OUTBACK): an international, open-label, randomised, phase 3 trial. Lancet Oncol. 2023;24(5):468–82. https://doi.org/10.1016/S1470-2045(23)00147-X.
9. Monk BJ, Toita T, Wu X, et al. Durvalumab versus placebo with chemoradiotherapy for locally advanced cervical cancer (CALLA): a randomised, double-blind, phase 3 trial. Lancet Oncol. 2023;24(12):1334–48. https://doi.org/10.1016/S1470-2045(23)00479-5.
10. Ai Y, Zhu H, Xie C, Jin X. Radiomics in cervical cancer: current applications and future potential. Crit Rev Oncol Hematol. 2020;152: 102985. https://doi.org/10.1016/j.critrevonc.2020.102985.
11. Bizzarri N, Russo L, Dolciami M, et al. Radiomics systematic review in cervical cancer: gynecological oncologist's perspective. Int J Gynecol Cancer. 2023;33(10):1522–41. https://doi.org/10.1136/ijgc-2023-004589.
12. Jha AK, Mithun S, Sherkhane UB, et al. Systematic review and meta-analysis of prediction models used in cervical cancer. Artif Intell Med. 2023;139: 102549. https://doi.org/10.1016/j.artmed.2023.1.
13. Manganaro L, Lakhman Y, Bharwani N, et al. Staging, recurrence and follow-up of uterine cervical cancer using MRI: updated guidelines of the European society of urogenital radiology after revised FIGO staging 2018. Eur Radiol. 2021;31(10):7802–16. https://doi.org/10.1007/s00330-020-07632-9.
14. Zhang X, Zhang Q, Chen Y, et al. MRI-based radiomics for pretreatment prediction of response to concurrent chemoradiotherapy in locally advanced cervical squamous cell cancer. Abdom Radiol (NY). 2023;48(1):367–76. https://doi.org/10.1007/s00261-022-03665-4.
15. Zhang X, Zhang Q, Guo J, et al. Added-value of texture analysis of ADC in predicting the survival of patients with 2018 FIGO stage IIICr cervical cancer treated by concurrent chemoradiotherapy. Eur J Radiol. 2022;150: 110272. https://doi.org/10.1016/j.ejrad.2022.110272.
16. Zhang X, Zhang Q, Xie L, et al. The value of whole-tumor texture analysis of ADC in predicting the early recurrence of locally advanced cervical squamous cell cancer treated with concurrent chemoradiotherapy. Front Oncol. 2022;12:852308. https://doi.org/10.3389/fonc.2022.852308.
17. Ikushima H, Haga A, Ando K, et al. Prediction of out-of-field recurrence after chemoradiotherapy for cervical cancer using a combination model of clinical parameters and magnetic resonance imaging radiomics: a multi-institutional study of the Japanese radiation oncology study group. J Radiat Res. 2022;63(1):98–106. https://doi.org/10.1093/jrr/rrab104.
18. Cai M, Yao F, Ding J, et al. MRI radiomic features: a potential biomarker for progression-free survival prediction of patients with locally advanced cervical cancer undergoing surgery. Front Oncol. 2021;11:749114. https://doi.org/10.3389/fonc.2021.749114.
19. Zhang Y, Liu L, Zhang K, et al. Nomograms combining clinical and imaging parameters to predict recurrence and disease-free survival after concurrent chemoradiotherapy in patients with locally advanced cervical cancer. Acad Radiol. 2023;30(3):499–508. https://doi.org/10.1016/j.acra.2022.08.002.
20. Autorino R, Gui B, Panza G, et al. Radiomics-based prediction of two-year clinical outcome in locally advanced cervical cancer patients undergoing neoadjuvant chemoradiotherapy. Radiol Med. 2022;127(5):498–506. https://doi.org/10.1007/s11547-022-01482-9.
21. Schmid MP, Lindegaard JC, Mahantshetty U, et al. Risk factors for local failure following chemoradiation and magnetic resonance image-guided brachytherapy in locally advanced cervical cancer: results from the EMBRACE-I study. J Clin Oncol. 2023;41(10):1933–42. https://doi.org/10.1200/JCO.22.01096.
22. Solomon D, Deeb AL, Tarabine K, et al. Predicting outcomes in esophageal adenocarcinoma following neoadjuvant chemoradiation: Interactions between tumor response and survival. J Thorac Cardiovasc Surg. 2023. https://doi.org/10.1016/j.jtcvs.2023.11.015.
23. Li X, Huang K, Zhang Q, et al. Early response to neoadjuvant chemotherapy can help predict long-term survival in patients with cervical cancer. Oncotarget. 2016;7(52):87485–95. https://doi.org/10.18632/oncotarget.11460.
24. Kong SY, Huang K, Zeng C, Ma X, Wang S. 2018 The association between short-term response and long-term survival for cervical cancer patients undergoing neoadjuvant chemotherapy: a system review and meta-analysis. Sci Rep. 2018;8(1):1545. https://doi.org/10.1038/s41598-018-19948-0.

Publisher's Note